Modeling links softening of myelin and spectrin scaffolds of axons after a concussion to increased vulnerability to repeated injuries

Aayush Kant[a,b], Victoria E. Johnson[c], John D. Arena[c], Jean-Pierre Dollé[c], Douglas H. Smith[c], and Vivek B. Shenoy[a,b,1]

[a]Center for Engineering Mechanobiology, University of Pennsylvania, Philadelphia, PA 19104; [b]Department of Materials Science and Engineering, University of Pennsylvania, Philadelphia, PA 19104; and [c]Penn Center for Brain Injury & Repair, Department of Neurosurgery, University of Pennsylvania, Philadelphia, PA 19104

Edited by David A. Weitz, Harvard University, Cambridge, MA, and approved May 23, 2021 (received for review December 14, 2020)

Damage to the microtubule lattice, which serves as a rigid cytoskeletal backbone for the axon, is a hallmark mechanical initiator of pathophysiology after concussion. Understanding the mechanical stress transfer from the brain tissue to the axonal cytoskeleton is essential to determine the microtubule lattice's vulnerability to mechanical injury. Here, we develop an ultrastructural model of the axon's cytoskeletal architecture to identify the components involved in the dynamic load transfer during injury. Corroborative in vivo studies were performed using a gyrencephalic swine model of concussion via single and repetitive head rotational acceleration. Computational analysis of the load transfer mechanism demonstrates that the myelin sheath and the actin/spectrin cortex play a significant role in effectively shielding the microtubules from tissue stress. We derive failure maps in the space spanned by tissue stress and stress rate to identify physiological conditions in which the microtubule lattice can rupture. We establish that a softer axonal cortex leads to a higher susceptibility of the microtubules to failure. Immunohistochemical examination of tissue from the swine model of single and repetitive concussion confirms the presence of postinjury spectrin degradation, with more extensive pathology observed following repetitive injury. Because the degradation of myelin and spectrin occurs over weeks following the first injury, we show that softening of the myelin layer and axonal cortex exposes the microtubules to higher stress during repeated incidences of traumatic brain injuries. Our predictions explain how mechanical injury predisposes axons to exacerbated responses to repeated injuries, as observed in vitro and in vivo.

axonal cytoskeleton damage | repeated traumatic brain injuries | cytoskeletal load transfer mechanism

The incidence of traumatic brain injury (TBI) has been consistently increasing globally, with a corresponding increase in the associated socioeconomic burden, especially in middle and low sociodemographic index countries (1). Up to 70 to 90% of TBI cases are mild, alternatively called concussion (2). Diffuse axonal injury (DAI), characterized neuropathologically by swollen axonal profiles across the white matter of the brain, is one of the most important and prominent pathologies in all severities of TBI and is thought to be a primary pathology in concussion (3). These swellings represent axonal transport interruption, with an accumulation of transported proteins.

A unique aspect of TBI is its mechanical nature arising from local mechanical stress peaks, occurring at a time scale of microseconds to milliseconds after the head impact. White matter axons are particularly vulnerable to injury under these mechanical loads, owing to their high organization in anisotropic tracts and their linear and uniform cytoskeletal architecture (4). This includes the stiffest component of the axon, microtubules (MTs), which form a core running along the length of the axon. The MTs are surrounded coaxially by a cortical sheath primarily composed of periodic actin rings arranged in conjunction with spectrin tetramers just below the axonal membrane, or the axolemma (5). Tissue stress leading to a mechanical rupture of MTs is observed in vitro during stretch injury of axons, causing an undulating morphology to develop at the site of MT breakage. Notably, these axon undulations have also been observed in vivo following TBI (6). We have previously demonstrated that the viscoelastic response of the MT-associated protein, tau, plays a key role in MT rupture by inducing high stress at its MT binding site under dynamic mechanical loads (7, 8).

The axonal cortex has also been suggested to play a role in stabilizing the MT core of the axons since spectrin deficient axons display prominent undulations after bending deformations (9, 10). These observations indicate that the mechanical stress waves traversing through the brain tissue during the primary injury impinge on the intraaxonal cytoskeleton via the cytoskeletal cortex. This assertion indicates that alterations in the mechanical constitution of the axonal cortex alter its axonal mechanoprotective behavior.

The complex neurochemical processes may induce chemomechanical alterations in the axonal cytoskeleton following the local mechanical stresses in axons even after mild TBIs (mTBIs). Such downstream pathologies, distinct from the instantaneous primary mechanical injury, often occur at a delayed stage, ranging from minutes to even days post-TBI, and are classified as secondary injuries (11). One important pathway includes stress-actuated accumulation of intracellular calcium leading to activation of calpain, a proteolytic enzyme with multiple substrates within the axon (11).

Significance

Growing evidence from in vitro studies suggests that the axonal cytoskeleton plays a mechanoprotective role in axon while under dynamic mechanical loads during a traumatic brain injury (TBI). Via computational modeling, we elucidate how perturbations in physical properties of the salient components of axonal cytoskeleton impact the intraaxonal load-bearing mechanism, potentially resulting in its failure. Immunohistochemical analyses of tissue from an in vivo model of TBI confirm the presence of cytoskeletal neurochemical degradation. In conjunction with the experiments, our model explains the clinical observation of exacerbated axonal pathology after repetitive TBIs. Insights from this work can help advance the understanding of the long-term impacts of single and repeated TBIs and identify potential therapeutic targets for improving axonal response to injury.

Author contributions: A.K., J.-P.D., D.H.S., and V.B.S. designed research; A.K., V.E.J., J.-P.D., and V.B.S. performed research; A.K., V.E.J., J.D.A., and V.B.S. analyzed data; and A.K. wrote the paper.

The authors declare no competing interest.

This article is a PNAS Direct Submission.

[1]To whom correspondence may be addressed. Email: vshenoy@seas.upenn.edu.

This article contains supporting information online at https://www.pnas.org/lookup/suppl/doi:10.1073/pnas.2024961118/-/DCSupplemental.

Published July 7, 2021.

The most prominent targets of calpain proteolysis are the αII-spectrin and βII-spectrin subunits of the spectrin tetramers in the axonal cortex. Indeed, the presence of spectrin breakdown products (SBDP), in particular αII-spectrin N-terminal fragment (SNTF), in patient biofluids such as cerebrospinal fluid (CSF), blood plasma, and serum is a promising diagnostic biomarker for mTBI and likely reflects the presence of DAI (12, 13).

Immunostaining of axonal profiles after a nonimpact rotational acceleration model of a single mTBI in swine exhibits SNTF immunoreactivity within 6 h postinjury (14). Morphological abnormalities of SNTF immunoreactive axons such as beading and fragmentation are further observed within 72 h postinjury, indicative of degeneration (Fig. 1 *A* and *B*). Such SNTF immunoreactivity, in association with a similar axonal morphology, is also commonly observed following severe TBIs in humans (14) (Fig. 1*C*). Such secondary spectrin degradations after mTBI will hamper the mechanoprotective role played by the axonal cortex. Further, these studies also motivate us to assert that the extent of spectrin degradation would correlate with the loss of mechanical properties, such as elasticity, in the axonal cortex.

In addition to the axonal cytoskeleton, extraaxonal myelin sheath has also been suggested to play a role in protecting axons. The mechanoprotective behavior of myelin sheath is evidenced by increased vulnerability and reduced functional recovery of unmyelinated axons compared to the myelinated subpopulation after an injury to the rat brain (16). Myelin content in brain tissue has been observed to correlate with tissue stiffness, further suggesting that myelin provides structural support to the axons (17). Damage to extraaxonal myelin sheath has been widely reported, even in mild forms of TBI (18). Degradation and disruption of the myelin sheath in the white matter of the brain is commonly observed up to 6 wk to 3 mo following TBIs (18, 15). Stretch injuries have also been reported to result in proteolysis of myelin basic protein (MBP), resulting in demyelination (19). mTBI in mice can result in a persistent loss of white matter integrity even up to 12 mo after the injury (20). Taib et al. (15) report that the myelin abnormalities in the white matter can have various ultrastructural features

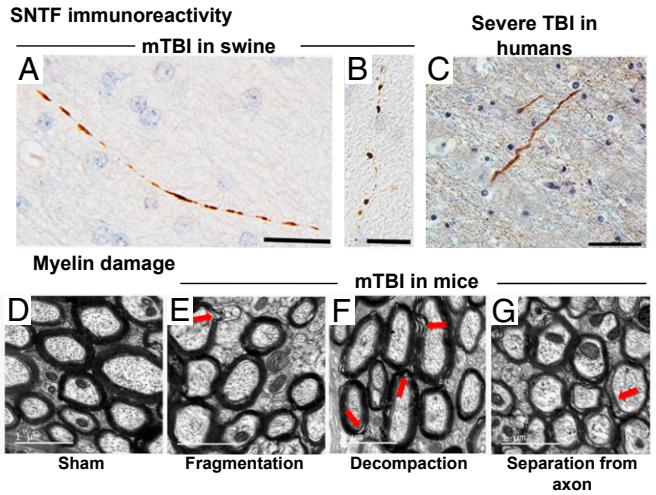

Fig. 1. A single SNTF positive axon in the subcortical white matter (*A*) 6 and (*B*) 72 h following a single mTBI in swine (14). (*C*) SNTF immunoreactive axon with an undulating morphology in the parasagittal white matter of a 59-y-old male, 4 d following a severe TBI caused by a fall (14). Myelin sheath morphology around axons (*D*) in a sham-operated mice and after mild TBI exhibiting abnormalities such as (*E*) fragmentation, (*F*) decompaction, and (*G*) separation from axon (15). (Scale bars: *A* and *B*, 25 μm; *C*, 50 μm; and *D*–*G*, 1 μm.) *A*–*C* are reprinted by permission from ref. 14. Springer Nature: *Acta Neuropathologica*, copyright 2015. *D*–*G* are reprinted from ref. 15, which is licensed under CC BY 4.0.

such as fragmentation, decompaction of the myelin sheath, or a separation of the myelin sheath from the axon resulting in a delaminated myelin layer (Fig. 1 *D*–*G*). These observations suggest that the mechanoprotective behavior of myelin is also disrupted after a TBI.

The postinjury proteolytic activity also leads to downstream hyperphosphorylation of tau proteins in the MT core, thereby inhibiting their MT binding functionality. Indeed, unbound hyperphosphorylated tau is found at elevated levels in patient biofluids (13, 11). Calpain-mediated and other pertinent intraaxonal cytoskeletal pathophysiologies, in turn, render the axon more vulnerable to subsequent TBIs. A history of repeated concussions or a single moderate to severe TBI has been associated with TBI-related neurodegeneration (TReND), of which chronic traumatic encephalopathy is one form. Notably, TReND commonly includes tauopathy, similar to that found in Alzheimer's disease (21). Since tau is selectively an axonal MT-associated protein, it has been suggested that progressive axonal pathology after TBI leads to tauopathy (22, 21).

Several computational models have been proposed to study the tissue-scale consequences of mechanical primary injuries after a TBI (23, 24). At a cytoskeletal level, there have been certain efforts to understand the mechanism of axonal stretching and resulting effects on the subaxonal MT assembly (7, 25). Additionally, the effect of molecular mechanisms such as MT polymerization dynamics (26, 27) and tau binding dynamics (8) have also been investigated. However, a mechanistic understanding of the supporting role played by the axonal cytoskeletal architecture, especially its chemomechanical modifications due to post-TBI neurodegeneration, is yet unexplored. Cytoskeletal proteolytic degradation in an axon during the secondary injury after a TBI is expected to elevate the axon's susceptibility to damage in the incidence of repetitive TBIs. Through this work, we develop a mathematical framework to establish that the myelin and the cytoskeletal cortex in the axon play a mechanoprotective role for the otherwise vulnerable MT core. We uncover how mechanical stresses from the brain tissue are transferred to the axonal MTs, which are implicated in axonal pathology. Based on this load transfer mechanism, we develop a failure locus predicting the space spanned by pertinent parameters wherein the MT rupture occurs. We further establish parametric regimes for tissue stress and stress rate where MTs rupture. Last, using our model, we develop a mechanistic understanding of the role played by neurochemical damage during secondary injuries in rendering the MTs mechanically more susceptible to repeated TBIs.

Methods

Mechanics of Load Transfer across the Cytoskeletal Architecture. To analyze the mechanism of load transfer in the axonal cytoskeletal assembly, we first study the ultrastructural arrangement of cytoskeletal proteins in the axon. Fig. 2*A* shows a three-dimensional schematic of a myelinated axon with an MT core and an outer cytoskeletal cortex. As shown in Fig. 2 *B* and *C*, individual MTs are held in a hexagonal arrangement via cross-linking proteins such as tau (7), while being uniformly staggered with respect to each other by half their lengths L [typically $2L = 2 - 10$ μm (28)]. Following a shear lag model (29), we assume that the deformation of cross-linkers (typically tau proteins) allows a transfer of shear forces between the elastic MTs [elastic modulus $E_m \sim 1.9$ GPa (30)] with a cross-section area A_M [~336.94 nm^2 (30)], while the MTs themselves withstand an axial tensile or compressive load. To capture their rate-dependent unfolding behavior (31), a Kelvin-viscoelastic model is assumed for the tau proteins with a spring of stiffness K_τ [~0.25 pN/nm (7)] in parallel to a dashpot with a viscous time scale η_t [~0.35 s (7)] as shown in Fig. 2 *D*, Left. The force F_τ–deformation δ_τ relationship for such a cross-linker is given as $F_\tau = K_\tau\{\eta_t\dot{\delta}_\tau + \delta_\tau\}$ where the dot represents a time derivative that lends a loading rate dependence to the axonal cytoskeletal architecture, a behavior commonly observed in vitro (7, 32). While shear-lag models traditionally assume an elastic cross-linker, a viscoelastic model is more consistent with the unfolding behavior of cross-linking proteins when they are stretched (31).

The axonal cortex composed of actin rings with spectrin tetramers (5) in conjunction with the myelin sheath tightly wrapped, without slip, around the axolemma (33) are together treated as a single elastic bilayer surrounding the

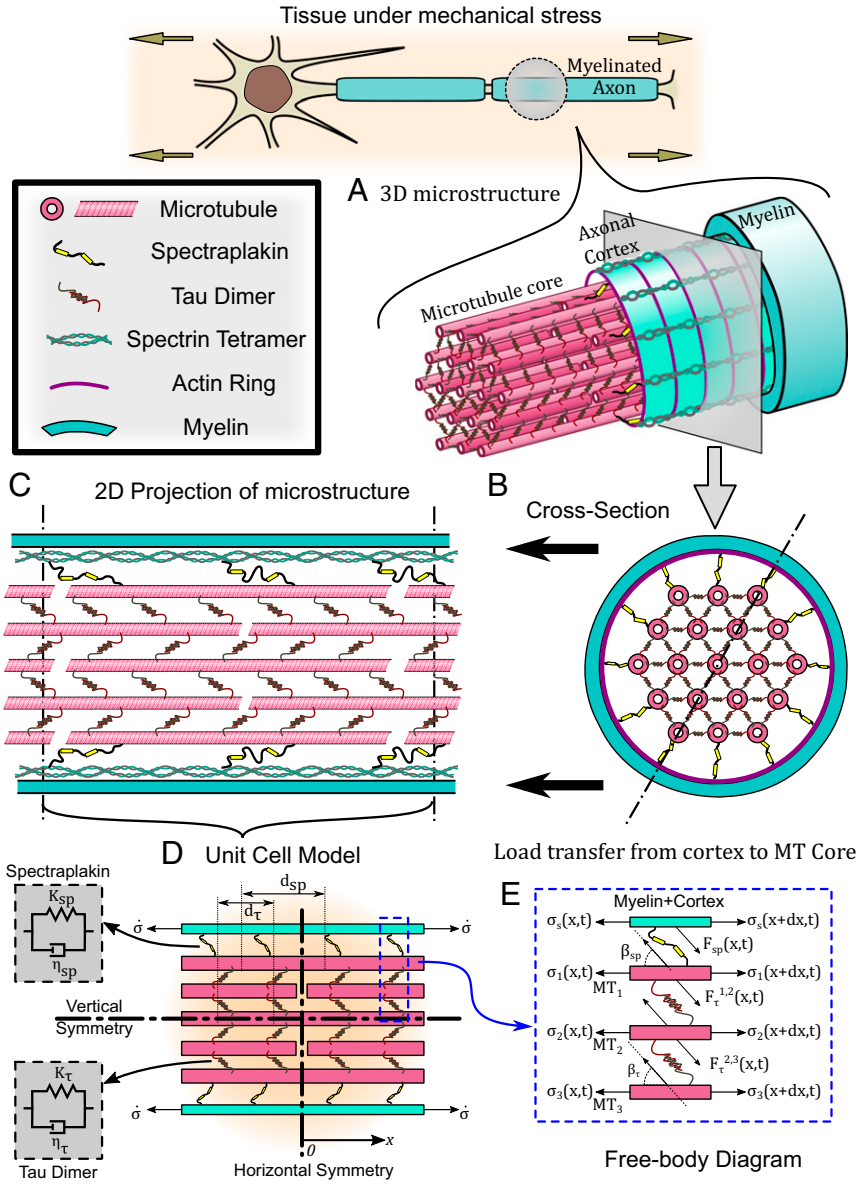

Fig. 2. A schematic diagram representing the cytoskeletal microstructure of an axon. (*A*) The axonal microstructure is composed of the actin/spectrin cortex surrounding the MT core. The MTs are cross-linked to each other by a tau protein dimer. The MT core is itself connected to the cortical cytoskeleton via spectraplakin cross-linkers. Additionally, the axon itself is surrounded by a protective myelin sheath. (*B*) A cross-section depicting the hexagonal arrangement of the MTs in the core surrounded by the axonal cortex and myelin. (*C*) A longitudinal cross-section depicting the staggered arrangement of the MTs in the core. The myelin sheath and axonal cortex are conjoined into a myelin-cortex bilayer. (*D*) (*Right*) The schematic of the unit cell model, which is used to mathematically capture the behavior of the axonal cytoskeleton under a cortical loading with a constant stress rate $\dot{\sigma}$. (*Left*) The cross-linking polymers spectraplakin and tau exhibit a viscoelastic material property captured by a Kelvin model of a spring and dashpot in parallel. The horizontal and vertical axes of symmetry in the unit cell are labeled. (*E*) Last, we apply a force balance of the axial and shear forces acting in the cytoskeletal proteins, as shown in the free body diagram.

MT core with an effective cross-sectional area A_s with an effective elastic modulus E_s (*SI Appendix*, Table S1). At the expense of adding additional parameters to the model, it is also possible that we can decouple the axonal cortex and myelin sheath into separate elastic layers which are linked via axon–myelin interaction proteins such as myelin-associated glycoproteins (34). In *SI Appendix*, Section S.2, we will extend our model to allow for a separate myelin and cortex and discuss the load transfer to the MTs as the coupling between them increases. We also show that under a no-slip boundary condition between the myelin and axon the decoupled model reduces to the coupled model we follow here.

The MT core and the myelin-cortex bilayer are interlinked via the spectraplakin family of proteins like dystonin, ACF7 (actin cross-linking family 7), and possibly other MT associated proteins (5) (stiffness K_{sp} and a viscous time scale η_{sp}), satisfying a force deformation equation similar to the tau proteins. The spacing between consecutive tau proteins is denoted by d_τ [typically ~30 nm (7)] and between consecutive spectraplakin as d_{sp} (*SI Appendix*, Table S1). It must be noted that since a uniform myelination over the axolemma is assumed, our model is suitable for capturing the axonal length between the nodes of Ranvier.

We define a unit cell of length $2L$ as shown in Fig. 2*D* such that by repeating it along the axonal axis, the cytoskeletal microstructure of the axon is generated. Let u_i be the elongation of MT_i and u_s be the elongation of the axonal cortex. Following the free body diagram in Fig. 2*E*, a balance of forces in the axial direction over an infinitesimal region of any MT gives the governing equation for that MT. Following this procedure for the cortex and each MT gives the equations governing the stress in cortex and the MTs as in *SI Appendix*, Eq. **S2**. The details on the derivation of the governing equation along with appropriate boundary and loading conditions can be found in

SI Appendix, Section S.1. Briefly, the cortex and alternate MTs are fixed at their midpoints to allow for staggered MT arrangement and the horizontal symmetry of the unit cell. A ramped tissue stress at a constant rate of $\dot{\sigma}$ is applied to the myelin-cortex bilayer. We solve *SI Appendix*, Eq. **S4**, for the cortical and MT displacement fields (u_s and u_i, respectively). A derivation of the governing equations and boundary conditions with rescaled coordinates along with additional details on the modeling description can be found in *SI Appendix*, Section S.1.

Immunohistochemistry. All experiments were conducted in accordance with protocols approved by The University of Pennsylvania Institutional Animal Care and Use Committee. Under general anesthesia, 6-mo-old female Hanford miniature swine underwent 1) repetitive rotational injuries performed 24 h apart with survival of 72 h from the first injury ($n = 3$), 2) single rotational injury with survival of 48 h ($n = 2$) or 72 h ($n = 3$) as previously reported (14) (selected to match the survival duration from both exposures in the repetitive group), and 3) shams ($n = 3$). Details on the swine mTBI procedure can be found in *SI Appendix*, Section S.3.

Whole-brain coronal, 8-μm-thick tissue sections from the animals were prepared for immunohistochemical examination at the level of the posterior hippocampus. Following deparaffinization and rehydration, tissue sections were immersed in aqueous hydrogen peroxide (15 min) to quench endogenous peroxidase activity. Antigen retrieval was performed in a microwave pressure cooker with immersion in preheated Tris EDTA buffer. Subsequent blocking was achieved using 1% normal horse serum (Vector Labs) in Optimax buffer (BioGenex) for 30 min. Incubation with the primary antibody was performed overnight at 4 °C. Specifically, sections were labeled with the antibody Ab2233 (rabbit: 1:17.5K) specific for the calpain-generated neoepitope at the carboxyl-end of the calpain-derived α-spectrin N-terminal fragment, SNTF (αII-spectrin residues 1 to 1176). The specificity of this cleavage site-specific antibody has been well established by Western blot, protease digest, and protease inhibitor studies (35–39). After rinsing, sections were incubated with the relevant species-specific biotinylated secondary antibody (Vector Labs), followed by avidin-biotin complex (Vectastain Universal Elite kit; Vector Labs). Visualization was achieved using 3,3′-diaminobenzidine (Vector Labs) and counterstaining with hematoxylin.

Positive control tissue included sections with previously established DAI. Omission of the primary antibody was performed on the same material to control for nonspecific binding.

Following immunostaining, tissue sections were subjected to high-resolution digital scanning at 20× magnification using the Aperio ScanScope for blinded review by two independent reviewers (V.E.J. and J.D.A.) using Aperio ImageScope software (Leica Biosystems).

Tissue sections were reviewed for SNTF+ immunoreactive profiles with morphologies consistent with traumatic axonal pathology as previously described in detail (14). Upon identification, SNTF+ profiles were manually tagged using the annotation tool in the Aperio ImageScope software, and the number of pathological axons was quantified per unit area across the entire subcortical white matter of both hemispheres in each whole brain coronal section. Groups were compared via one-way ANOVA with multiple comparisons using GraphPad Prism (GraphPad Software).

Results

Axonal Cortex and Myelin Shield the MT Core. As discussed in *Mechanics of Load Transfer across the Cytoskeletal Architecture*, during a TBI the tissue experiences dynamic loads which are captured by applying a ramped tissue stress, $\dot{\sigma}$, to the myelin layer and axonal cortex directly in contact with the tissue. We then study the mechanisms of transfer of the extraaxonal tissue stress to the MT bundle at the core of the axon. Since the load transfer from the tissue to the MT core occurs via the myelin-cortex bilayer and the spectraplakin linkers, parameters such as stiffness and viscosity of linkers, their spatial density, and cortical elasticity are expected to play a significant role on the extent of load transfer. The governing equation (*SI Appendix*, Eq. **S4**) incorporates the roles of these parameters via six nondimensional ratios listed in *SI Appendix*, Table S1. Of these, the nondimensional MT half-length, L/L_c, and the relative cortical cross-sectional area, A_s/A_M, can be estimated from published studies (28, 30, 40). As MTs are considered to be the stiffest components of the axonal cytoskeleton (6), the stiffness of the myelin-cortex bilayer is estimated to be two orders of magnitude smaller, $E_s/E_M = 0.01$. Also, it has been suggested that stiff cross-linking permits the MT lattice to tolerate higher compressive forces (5). While it has been shown that the actin–MT composites with actin–MT cross-linking exhibit slightly lower stiffness than composites with MT–MT cross-linking (41), there are no published reports which conclusively establish the stiffness of the actin–MT cross-linkers like spectraplakin relative to MT–MT cross-linkers like tau. However, we estimate that a relatively relaxed cortex–MT cross-linking as compared to the MT–MT cross-linking will reduce the extent of tissue stress transferred to the MTs. Thus, we choose the following range of parametric ratios: $0.25 < K_{sp}/K_\tau < 1$, $0.25 < \eta_{sp}/\eta_\tau < 1$, and $1 < d_{sp}/d_\tau < 10$. We now study how alteration in the magnitudes of these dimensionless parameters alters the level of extraaxonal forces transmitted to the MT.

Softer axonal cortex and myelin sheath increase the load transfer to MTs. Since tissue stress is transferred to the intraaxonal cytoskeleton via the myelin sheath and the axonal cortex, the stiffness of the myelin-cortex bilayer is expected to play an important role in the transfer of tissue stress to the MT core. In presence of axonal loads discussed in *Mechanics of Load Transfer across the Cytoskeletal Architecture*, we note that the myelin sheath and the axonal cortex act analogous to two elastic elements in parallel. Thus, the effective stiffness of the myelin-cortical bilayer is the sum of the individual stiffnesses of the myelin and the cortex. The role played by the effective myelin-cortical stiffness becomes especially crucial due to the secondary injuries after TBI, wherein the neurochemical degradation of the cortical cytoskeleton and myelin occurs.

We, therefore, evaluated the MT stress predicted by the model upon decreasing the relative cortical elastic modulus (E_s/E_M) from 0.02 to 0.005. As the myelin-cortex bilayer becomes soft, we expect it to stretch easily, increasing the cortical deformation, u_s, which results in a higher spectraplakin elongation, $u_s - u_1$. Thus, the force transferred across the spectraplakins $[= K_{sp}(u_s - u_1)]$ increases, resulting in higher stress in the MT. As seen from Fig. 3, schematics 1 and 2, when the cortex becomes soft, increased load transfer across the spectraplakin increases the MT stress. For the same tissue stress, the MT stress is higher for a softer cortex or myelin sheath indicating a likelier occurrence of MT lattice rupture. A softer cortex or myelin sheath, therefore, would have debilitating effects on MT stability, effectively resulting in the loss of MT shielding. It must be noted that for maximum axonal shielding (least load transfer to MTs), both the cortex as well as the myelin must be intact. Degradation of either of these components of the bilayer would result in loss of bilayer stiffness. The results derived here will be used in *In Vivo Observations on Role of Spectrin and Myelin after mTBI* to capture the effect of proteolytic degradation of the axonal cortex and the myelin sheath on the transfer of tissue stress to the MT core.

The parameters governing the MT–cortex spectraplakin cross-linkers—relative spectraplakin stiffness (K_{sp}/K_τ), relative spectraplakin viscosity (η_{sp}/η_τ), the relative spectraplakin spacing (d_{sp}/d_τ), and the length of the MTs (L/L_c)—also play an important role in the transfer of tissue stress to the MT core. The roles played by these parameters are discussed in detail in *SI Appendix*, Section S.3. The parametric space for model parameters governing the cortex (elasticity vs. cross-sectional area), the spectraplakin (stiffness vs. relative spacing), and the MT length are also explored by performing a sensitivity analysis on the model (*SI Appendix*, Section S.3). Taken together, these results indicate that for a given tissue stress, the constitutive parameters governing the stress deformation response of the cytoskeletal components, as well as the geometric parameters governing the cytoskeletal architecture, determine the extent of load transferred from the external tissue to the MT core. In this section, we have kept the stress rate constant to exclude studying the effects of dynamic loading. In the next section, we improve this study by varying the tissue stress rate.

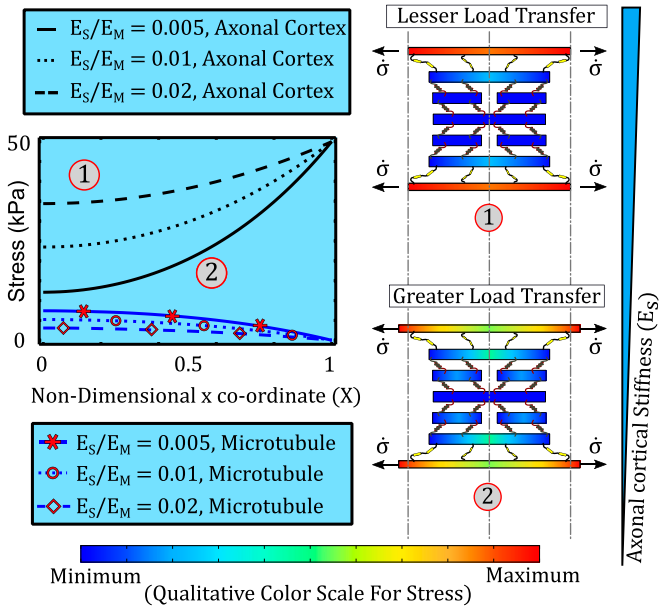

Fig. 3. The effect of cytoskeletal cortical stiffness on the spatial variation of the stress in spectrin (black, no markers) and in MT (blue, with red markers) over the length of the half unit cell. As the ratio of cortical stiffness to MT stiffness increases from 0.005 to 0.02, MT stress reduces due to reduced load transfer by stiffer cortex. Schematics 1 and 2 display the effect of reducing cortical stiffness on the load transfer and cortical elongation.

MTs Are Sensitive to the Tissue Loading Rate. Concussions occur due to head impacts at very high loading rates with brain tissues reaching peak rotational accelerations in excess of 8,000 rad/s^2 within 10 ms of impact (42) and local tissue stresses of around 50 kPa (43, 23). The axonal cytoskeleton is sensitive to not just the external loads but also the rate of application of load (32) with a strain softening behavior of axons under stretch indicative of its viscoelastic nature (44). Thus, we investigate the effect of changing the tissue stress rate on the load transfer to the MT lattice.

We reduce the duration of ramped tissue stress from 50 ms (corresponding to a stress rate of 1 kPa/ms [$\dot{\sigma}\eta_\tau/\sigma_{max} = 7$]) to 10 ms (corresponding to 5 kPa/ms [$\dot{\sigma}\eta_\tau/\sigma_{max} = 35$]). We consider an additional case of quasi-static loading where the ramping duration is very long (~ 35 s) such that $\dot{\sigma}\eta_\tau/\sigma_{max} = 0.01$. Our model predicts that with increasing tissue stress rates, the extent of load transfer from the cortex to the MT lattice increases resulting in higher MT stresses (*SI Appendix*, Fig. S5). It can be seen that at higher loading rates the rate of deformation ($\dot{\delta}_{sp}$) of the viscoelastic spectraplakin increases thereby transferring greater force (as per *SI Appendix*, Fig. Eq. **S1**) to the MTs, effectively making the spectraplakin stiffer at a higher stress rate. Having observed that the axon's vulnerability to MT rupture at a given tissue stress is influenced by the applied loading rate of the tissue stress, we next try to assess the tissue loading regimes that can lead to axonal damage.

To explore the possible physiological loading regimes, we present a phase diagram depicting the safe/unsafe parameter space for the two tissue loading parameters, the tissue stress ($\dot{\sigma}t$) and the nondimensional tissue stress rate ($\dot{\sigma}\eta_\tau/\sigma_{max}$), in Fig. 4*J*. Here let us consider the case when the axonal cortex stiffness is at its physiologically unaltered value ($E_s/E_{MT} = 0.01$) as depicted in yellow in Fig. 4*J*. The unsafe parameter space, depicted by the yellow region, and the safe parameter space, outside the yellow region, are separated by a yellow curve along which the MT stress reaches an assumed critical threshold of 7 kPa. The yellow curve, therefore, denotes the locus of critical tissue stress (on the *x* axis of the phase diagram), which can be tolerated as the tissue stress rate (on the *y* axis) increases while axonal cortical elasticity is unaltered (Fig. 4*J*). Therefore, while for low stress rates, high tissue stresses can be tolerated by the axon, at higher stress rates, the tissue stress which can be tolerated by the axon declines. For high loading rates (~5 kPa/ms, $\dot{\sigma}\eta_\tau/\sigma_{max} = 35$), critical MT stress of 7 kPa is reached at tissue stresses of ~ 40 kPa. This corresponds to a tissue stress of 40 kPa being reached in a duration of 8 ms, a loading condition similar to those predicted to result in concussive injuries (43, 23). In *Incorporating the Effects of Real-Life Post-TBI Spectrin and Myelin Proteolysis in the Computational Model*, we further develop this phase diagram to show the evolution of the unsafe parameter space as the cortical elasticity is altered.

The model predictions discussed in *Axonal Cortex and Myelin Shield the MT Core* and *MTs Are Sensitive to the Tissue Loading Rate* clearly enunciate the role played by the axonal cytoskeleton in shielding the MTs under dynamic loading conditions similar to the physiological loads during an mTBI. Of interest are the shielding effects of the axonal cortex and the myelin sheath. As such, proteolytic degradation of spectrin within the axonal cortex and MBP in the myelin sheath could therefore be expected to play a significant role in making the axons more vulnerable to injuries after a TBI has already occurred. In the next sections, we explore experimentally the role of spectrin and myelin degradation in single and repeated mTBIs.

In Vivo Observations on Role of Spectrin and Myelin after mTBI. Following concussion in vivo, gross neuropathological examination of the swine brain revealed no differences between injured and sham animals. Specifically, there was no evidence of any focal hemorrhagic or ischemic lesions. In addition, there was no evidence of brain swelling or raised intracranial pressure, with both hemispheres being symmetrical and without midline shift.

In a previous report we demonstrated immunoreactivity specific for SNTF (SNTF+) in axons with an injured morphology at 48 and 72 h following a single mTBI exposure in the rotational model (14). Here comparisons of tissue from these studies were performed in parallel with those following repeat mTBI exposures. Direct quantification within the white matter revealed notably more extensive SNTF+ axonal pathology [2.03±0.12(SEM) profiles per mm^2] with repetitive injury versus just single rotations at both 48 h [0.49±0.17(SEM) profiles per mm^2; $P = 0.003$] and 72 h [0.91±0.27(SEM) profiles per mm^2; $P = 0.03$] survival. Notably, only very minimal or no SNTF+ injured axons were observed in sham animals [all score 0.09±0.08(SEM) profiles per mm^2].

Individual data are shown in Fig. 4. SNTF+ axons were notably observed in anatomic regions, including the periventricular white matter, previously observed to have a high burden of pathology in this model using gold-standard markers of DAI (14, 45). This was consistent with both single and repeat injury models, and the multifocal and biomechanical distribution of pathology reflects regions of high strain experienced at the instant of trauma.

Morphologically, individual SNTF+ axons displayed small swellings, often with a beaded appearance along the axon length (Fig. 4 *D*–*H*). In addition, more isolated SNFT+ profiles could be observed, likely reflecting single points of cytoskeletal disruption or terminal disconnection (Fig. 4 *F* and *H*). Notably, these findings were consistent with reported descriptions of SNTF immunoreactive axons in brain tissue following severe TBI in humans (14) indicating clinical relevance (Fig. 1*C*). Interestingly, following repeat injuries, small clusters of SNTF+ profiles were frequently observed, particularly in the periventricular region, potentially representing a high degree of axon fragmentation and degeneration when compared with single mTBI. This increased fragmentation may in part account for the increased number of profiles demonstrated in Fig. 4.

Together these data confirm the presence of calpain-mediated spectrin breakdown within traumatically injured axons in vivo after single and repeated mTBIs. Moreover, the extent and pathological morphologies of injured axons were more frequent following

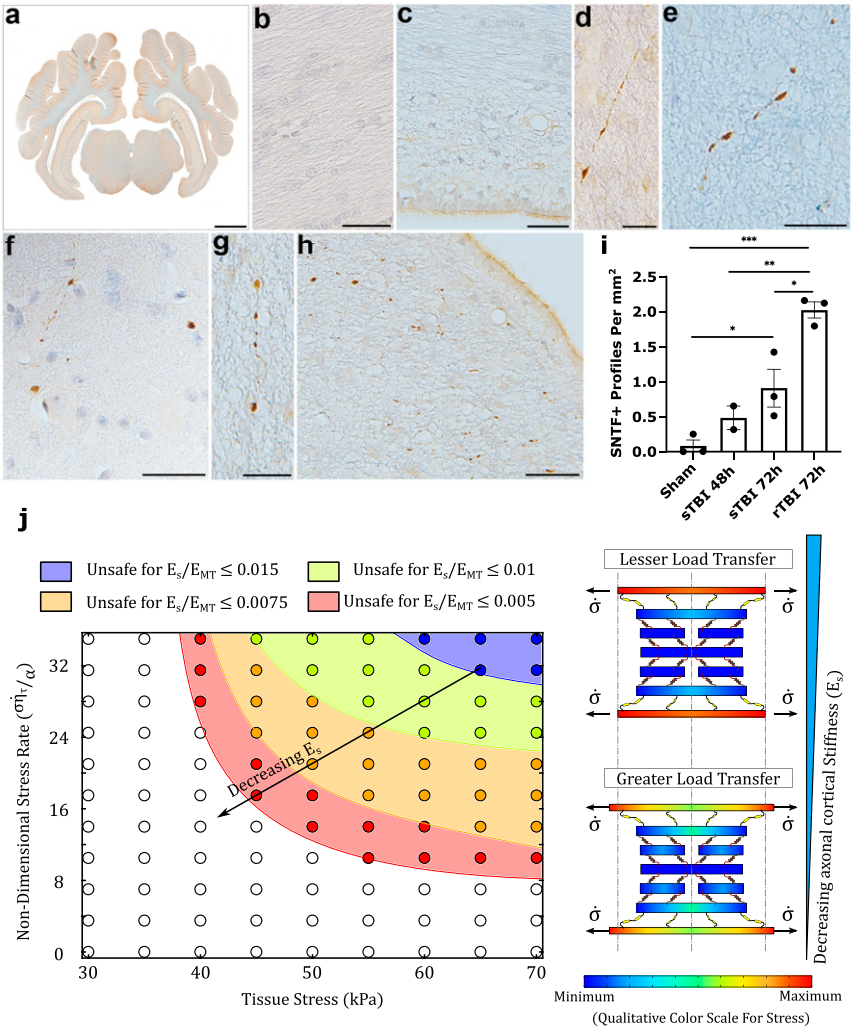

Fig. 4. (*A*) Representative example of the brain region examined (whole-brain tissue section in the coronal plane at the level of the posterior hippocampus). (*B* and *C*) Regions of white matter in sham animals showing an absence of SNTF immunoreactivity, including directly adjacent to the lateral ventricle (*C*). (*D*) SNTF+ axon in the periventricular white matter showing multiple small swellings along its length at 48 h following a single rotational injury. (*E*) SNTF+ axon with bead-like morphology within the white matter at 72h following a single rotational injury. (*F–H*) Multiple SNTF+ axonal swellings in the white matter, including the periventricular white matter following repeat rotational injuries (72 h survival from the first injury). (*I*) Quantification of the number of SNTF+ axonal profiles per mm^2 displaying morphological features of injury in shams versus 48 and 72 h after a single rotational injury and 72 h after repeated rotational injuries. *P* values reported as $*P < 0.05$, $**P < 0.01$, $***P < 0.001$. (*J*) Phase diagram illustrating the safe/unsafe parameter space for the loading parameters tissue stress and corresponding nondimensional stress rate for various ratios of spectrin stiffness to MT stiffness (E_s/E_{MT}). For all the parameters it is seen that a combination of high stress and stress rate leads to MT failure. The direction of arrow indicates a growing unsafe parameter space with decrease in cortical elasticity. The schematic diagram to the right depicts the effects of the spectrin stiffness on the load transfer in the cytoskeletal unit cell. A softer cortex elongates more, allowing a higher transfer of stresses to the MTs via the spectraplakin. (Scale bars: *A*, 7 mm; *B*, *C*, *F*, and *H*, 50 μm; and *D*, *E*, and *G*, 25 μm.)

repetitive injury and corroborate the model predictions regarding the mechanoprotective role of spectrin. Our model predictions discussed in *Axonal Cortex and Myelin Shield the MT Core* and *MTs Are Sensitive to the Tissue Loading Rate* explain how the dynamic tissue loads are transferred to the MTs resulting in their rupture. Next, we use the results from our experiments, as well as those previously reported in literature, to quantitatively explain why such long-term secondary pathologies after a TBI would increase the vulnerability of the axon to future TBIs.

From a mechanobiological perspective, as the spectrin in the axonal cortex is proteolyzed into SNTF fragments, it can be expected that the structural rigidity of the axonal cortical assembly made up of actin rings interconnected with spectrin tetramers is compromised. Therefore, in the model, we can capture the effects of calpain-mediated proteolytic breakdown of spectrin by reducing the cortical elasticity. As discussed in *MTs Are Sensitive to the Tissue Loading Rate* the phase diagram in Fig. 4*J* shows the tissue loading regime (tissue load vs. loading rate) where the MTs are vulnerable. We consider a situation where a TBI has already happened, and secondary injuries following the TBI have resulted in spectrin proteolysis thereby reducing the elasticity of the axonal cortex. Assuming that the cortical elasticity has gone down by 25% (orange region in Fig. 4*J*), we see that the loading conditions (all orange circles) which were safe when the cortical elasticity was unaltered during the first TBI are now rendered unsafe. That is, if a second TBI occurs while the axonal cortex is in such a compromised condition, a much higher load would be transferred to the MTs, making it easier for them to rupture. In a similar fashion, if the cortical elasticity was even further compromised (say up to 50% in the red region), the vulnerability of the MTs would further be increased, and even lower tissue stress and stress rates would result in a MT rupture. Thus, our experimental observations are

in direct confirmation with our model prediction that breakdown of spectrin in the axonal cortex should increase the vulnerability of MTs to future injuries.

In this section the cortical elasticity is varied by an arbitrary amount to confirm the experimental findings. Next, we compare our model with previously reported levels of myelin and spectrin degradation in the axon in order to more accurately predict the increased axonal vulnerability after real-life TBI incidences.

Incorporating the Effects of Real-Life Post-TBI Spectrin and Myelin Proteolysis in the Computational Model. As discussed previously, secondary injuries following the mechanical impact during a TBI can induce degenerative proteolysis of cytoskeletal proteins as well as degradation of the myelin sheath, which we can functionally capture by evolving our model parameters such as the myelin-cortical bilayer elasticity. Such functional variation in the values of model parameters can be used to accurately predict an altered vulnerability of the MT lattice to repeated incidences of TBI.

Spectrin degradation increases axon vulnerability. The spectrin tetramers in the cytoskeletal cortex are composed of αII-spectrin subunits, which are susceptible to proteolysis by activated calpain following intracellular calcium ion accumulation after a TBI. Clinically, mild as well as severe TBIs in patients have been associated with increase in blood, serum, and CSF SBDP such as SNTF (12, 46). Siman et al. (46) tested serum SNTF from ice hockey players experiencing a concussion. They reported the quantitative increase in serum SNTF at different times after the injury until their return to play, as reproduced in Fig. 5*A*. As a first approximation, we assume that at all time points, the elasticity of the myelin-cortex bilayer is reduced by a percentage linearly proportional to the increase in the serum SNTF. The many spectrin tetramers which link two neighboring actin rings in the axonal cortex are analogous to many springs acting in parallel, such that their effective stiffness is the sum of individual spectrin tetramers. When some of the αII spectrin proteins are proteolyzed into fragments, we can imagine they no longer contribute to the effective stiffness of the ultrastructure, effectively reducing it. As a first-order approximation we assume this to be a linear reduction. We utilize the quantitative observations by Siman et al. (46) to functionally approximate a reduction in the elastic modulus of the axonal cortex and thus predict the transfer of tissue stress in the event of a repeated brain injury.

Specifically, we chose four cases when a TBI occurs—first TBI when SNTF is at its baseline levels (blue in Fig. 5*A*), a second injury 1 h after the first (orange), a second injury 12 h after the first (red), and a second injury after the player returns to play (light blue hatched). For the first injury, the cortical elasticity is at its baseline level, and we find that the MTs experience maximum stress of 6.41 kPa. Due to calpain proteolysis during secondary injury, the cortical elasticity starts reducing. One hour after the first injury, the serum levels of SNTF rise by ~1.66 times which we interpret as a 13.2% reduction in cortical elasticity, as a first-order approximation. For this injury, an elevated peak MT stress of 6.85 kPa, nearly a 7% increase in MT stress, is observed in the MTs. If the second injury occurs 12 h after the first, per the data from Siman et al. (46), a 22.5% decrease in cortical elasticity is incorporated, resulting in an increase of peak MT stress to 7.18 kPa, higher than the threshold level. Increased serum SNTF is observed to persist at a similar level till up to 6 d after the first injury. Thus, according to our model, an incidence of a second injury up to 6 d after the first would elevate the MT stress above the threshold levels, resulting in axonal damage via MT rupture. Siman et al. (46) further note that at the time of player's return to play, the serum SNTF nearly returns to its baseline levels (~ 4.4% change from baseline). This indicates a recovery of spectrin in the axonal cortex and could be associated with reduced activation of calpain at such periods after injury. If the second injury occurs after the players return to play, the MT

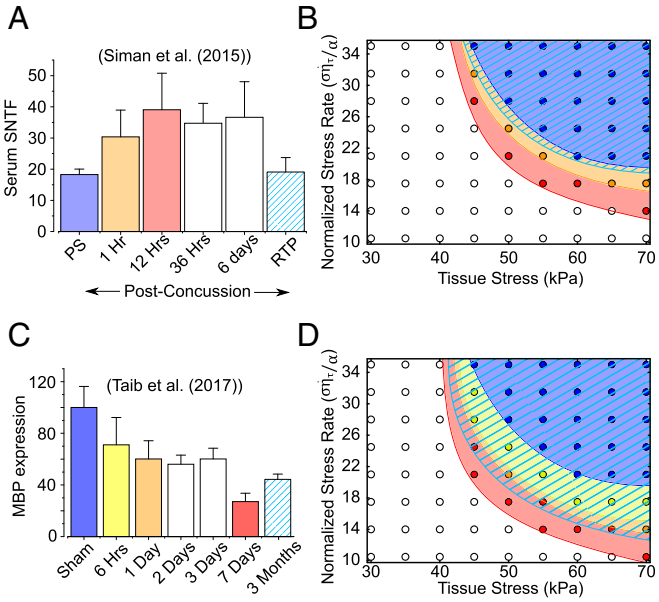

Fig. 5. The effect of cytoskeletal degradation during secondary injuries on repeated TBIs. (*A*) Quantitative assessment of serum SNTF levels by Siman et al. (46). We functionally reduce the cortical elasticity proportionally to the reported increase in serum SNTF 1 and 12 h after an mTBI and after the player's return to play. (*B*) The tissue stress–stress rate phase diagram illustrating the growing unsafe space (colored region) for repeated TBIs. When a second TBI occurs 1 and 12 h after the first TBI, the unsafe parametric space progressively grows from the blue to orange and finally to the red region. When a second TBI occurs after the return to play, the unsafe parametric space is seen to shrink to the hatched light blue region, indicating the player's recovery. The parametric coordinates (tissue stress and stress rate), which were safe for the first TBI, are no longer safe for repeated TBIs until the player's recovery. (*C*) Similar to spectrin degradation, we incorporate the role played by myelin damage in increasing the vulnerability of axon to repeated TBIs. Reduction in MBP expression in the contralateral corpus callosum of a sham-operated and TBI mice 6 h (yellow), 1 d (orange), 1 wk (red), and 3 mo (light blue hatched) after the first TBI as reported by Taib et al. (15). (*D*) The evolution of unsafe loading parameter space on the stress–stress rate phase diagram at each of the time points. By 3 mo, improvement in MBP expression is seen, resulting in shrinking of the unsafe loading parameter space (hatched light blue region).

stress would increase to only 6.43 kPa, well below the MT injury threshold.

Thus, based on the data reported by Siman et al. (46), our model presents a mechanistic explanation as to why a repetition of TBI between 1 h to 6 d of the first injury results in an increased axonal vulnerability to concussive injuries. However, by the time the player returns, the extent of spectrin breakdown is substantially reduced, such that if a second TBI occurs, the stress in MTs would be comparable to the first TBI and not exceed the injury thresholds. With this information at hand, we can now modify the stress–stress rate phase diagram from Fig. 4*A* to incorporate the reduction in cortical elasticity 1 and 12 h after the first injury. Fig. 5*B* shows the new phase diagram with the failure loci for the first injury (blue), followed by separate incidences of TBI 1 h (orange) and 12 h (red) after the first injury. The MT failure parameter space grows as the cortical stiffness reduces so that the tissue stress–stress rate parameter space, which was safe for the uninjured cortex, is no longer safe for the softer cortex 1 or 12 h after the first injury. In other words, the tolerable tissue stress reduces for the softer cortex, even if the loading conditions, the tissue stress and stress rate, stay unchanged. However, once the player has sufficient time to recuperate before returning to play,

the MT failure parameter space (light blue hatched) returns to the initial levels indicating an almost complete recovery.

Myelin degradation increases axon vulnerability. The expression of MBP is observed to be reduced due to damage to myelin-producing oligodendrocytes or via calpain proteolysis (19, 15, 47). Taib et al. (15) measured the reduction of MBP expression in the corpus callosum of mice up to 3 mo after a mild TBI. Since tissue stiffness has been suggested to scale approximately linearly with increasing myelin content (17), we assume that the stiffness of the myelin-cortex bilayer through which tissue stress is transferred to the axons also linearly reduces with a reduction in MBP expression. We utilize the quantitative observations by Taib et al. (15), as reproduced in Fig. 5*C*, to predict the transfer of tissue stress in the event of a repeated brain injury.

We chose five cases when a TBI occurs—first TBI when MBP expression is at its baseline levels (blue in Fig. 5*C*), a second injury 6 h after the first (yellow), a second injury 1 d after the first (orange), a second injury 1 wk after the first (red), and a second injury 3 mo after the first (light blue hatched). As in the previous section, for the first injury, the cortical elasticity is at its baseline level, and the MTs experience maximum stress of 6.41 kPa. Six hours after the injury, the MBP expression reduces to 71% of its uninjured level, such that the incidence of a second TBI at this stage leads to an increased MT stress of 6.90 kPa. A further reduction in MBP expression to 60.4% 1 d after the TBI results in the peak MT stress reaching 7.08 kPa, exceeding the threshold tolerable MT stress indicating that MT lattice will be damaged. One week after the TBI, the MBP expression further reduces to 27.3% leading to an even increased MT stress of 7.71 kPa. The vulnerability of the MT lattice to damage due to the second injury persists even up to 3 mo as the MBP expression is still reduced to 44.7% leading to MT stress of 7.37 kPa. Thus, in contrast to the axon vulnerability due to spectrin degradation which persists up to 3 d, our model predicts that due to MBP proteolysis the axons stay vulnerable for up to 3 mo after the first TBI.

Like in the previous section, the stress–stress rate phase diagram can be modified to incorporate the reduction in elasticity of the myelin-cortex bilayer up to 3 mo after the first TBI. Fig. 5*D* shows the new phase diagram with the failure loci for the first injury (blue), followed by separate incidences of TBI 6 h (yellow), 1 d (orange), 1 wk (red), and 3 mo (light blue hatched) after the first injury. Again, the MT failure parameter space grows as the bilayer stiffness reduces so that the tissue stress–stress rate parameter space, which was safe for the uninjured axon, is no longer safe with a softer bilayer after the first injury. A further 3 mo postinjury, the MBP expression shows a partial improvement, which is indicated by a reduction in the MT failure parameter space, although it has not yet reached its uninjured state.

Discussion

We have developed an ultrastructural model of the axon to better understand the mechanism of load transfer from the axonal cortex to the MT assembly at the axon's core. Our model incorporates an MT core, with a uniformly staggered hexagonal MT distribution cross-linked by viscoelastic tau proteins, surrounded by a relatively soft cytoskeletal cortex, composed of actin rings and spectrin tetramers, conjoined with the extraaxonal protective myelin coat. The viscoelastic linkers, spectraplakin, connect the axonal cortex to the MT core. We found the following:

1. As either the applied tissue stress or loading rate increases, the MT stress increases, increasing the chances of MT core rupture. Under quasi-static loading, the axons can withstand much larger stress.
2. Shorter MTs can withstand a much higher load than longer MTs.
3. A more effective MT shielding is observed for softer, less viscous spectraplakin linkers.
4. A sparser distribution of spectraplakin shields the MT. An important caveat, however, is that with too few linkers, the force across them can increase, leading to individual linker failure.
5. Last, but most significantly, we note that a softer myelin-cortex bilayer deforms more under a given stress, thereby transferring more load across the spectraplakin to the MT core. This can be immediately understood by imagining an infinitely stiff cortex, which will not deform, resulting in a zero spectraplakin elongation and no stress in the MTs. A stiffer cortex, therefore, acts as a shield protecting the MT core.

These results encapsulate the role played by individual axonal components, namely, the myelin sheath, actin–spectrin cortex, and the spectraplakin proteins in altering the extent of transfer of tissue stress to the otherwise vulnerable MT core. The model predictions indicate the existence of a parameter space where the cytoskeletal load transfer from the neuronal tissue to the intraaxonal MT core is optimized for an axon's ability to withstand the day-to-day stresses. These predictions give an indication of the effect of secondary injuries and related chemical degradation on axon's cytoskeletal load transfer mechanism. Further, the predictions from the model can also be used to identify key therapeutic targets such as spectraplakin, axonal cortex, or the extracellular myelin which can shield the axonal MTs otherwise susceptible to strain-induced during after TBI.

The chemical injury that follows the primary mechanical injury can alter the mechanoprotective behavior of cytoskeletal proteins via the activation of proteases. Whereas the primary mechanical injury occurs over microseconds to milliseconds, the chemical injury unfolds within minutes to hours and can persist for months (11). Since studies have shown that myelin content in the white matter directly correlates to tissue stiffness, and unmyelinated axons are more vulnerable and show larger functional deficits than myelinated axons following an experimental TBI (16, 17), it can be argued that axonal myelin provides some level of mechanoprotection from the initial primary mechanical injury. Studies have shown that stretch-induced injuries result in an increase in calcium ion concentrations in mature oligodendrocytes resulting in a reduction in MBP (47), likely due to the fact that MBP is a proteolytic substrate for calpain (19). This degradation/softening of the myelin component of the bilayer is commonly observed following a TBI, with delaminating and collapsed myelin observed within 3 d and axon and white matter degeneration observed to persist for months to years after a TBI in pigs and humans (18, 15, 48). The primary mechanical injury also injures oligodendrocytes, which can either lead to cell death or significantly affect myelin turnover that is constantly occurring (18). Compensating for the drop in mature oligodendrocytes, increases in oligodendrocyte progenitors have been observed, although the resulting remyelination is characterized by a reduction in myelin sheath thickness (49).

In addition to the breakdown of MBP, the protease calpain has been consistently reported to play a significant role in the proteolysis of the cytoskeletal protein spectrin in the axonal cortex after a TBI (50, 51). Spectrin is an important component of the axonal cytoskeleton linking the axolemma to actin within the axon cortex and regulating the transmission of externally applied mechanical forces (9, 10). Axon's strain-softening behavior has been attributed to the unfolding of spectrin repeats, enabling it to act as a shock absorber (44), and axons lacking spectrin break easily when exposed to mechanical strains (52). Breakdown of αII-spectrin results in SBDPs that can be detected in blood serum as a direct consequence of proteins being released from degenerating neurons (13). In particular, measurement of serum SNTF may have utility in both diagnosis and prognosis of mTBI (46). SBDPs were also significantly elevated in the CSF of patients following severe TBI and were found to correlate with outcome (12). Moreover, immunohistochemistry specific for SNTF can identify DAI in brain

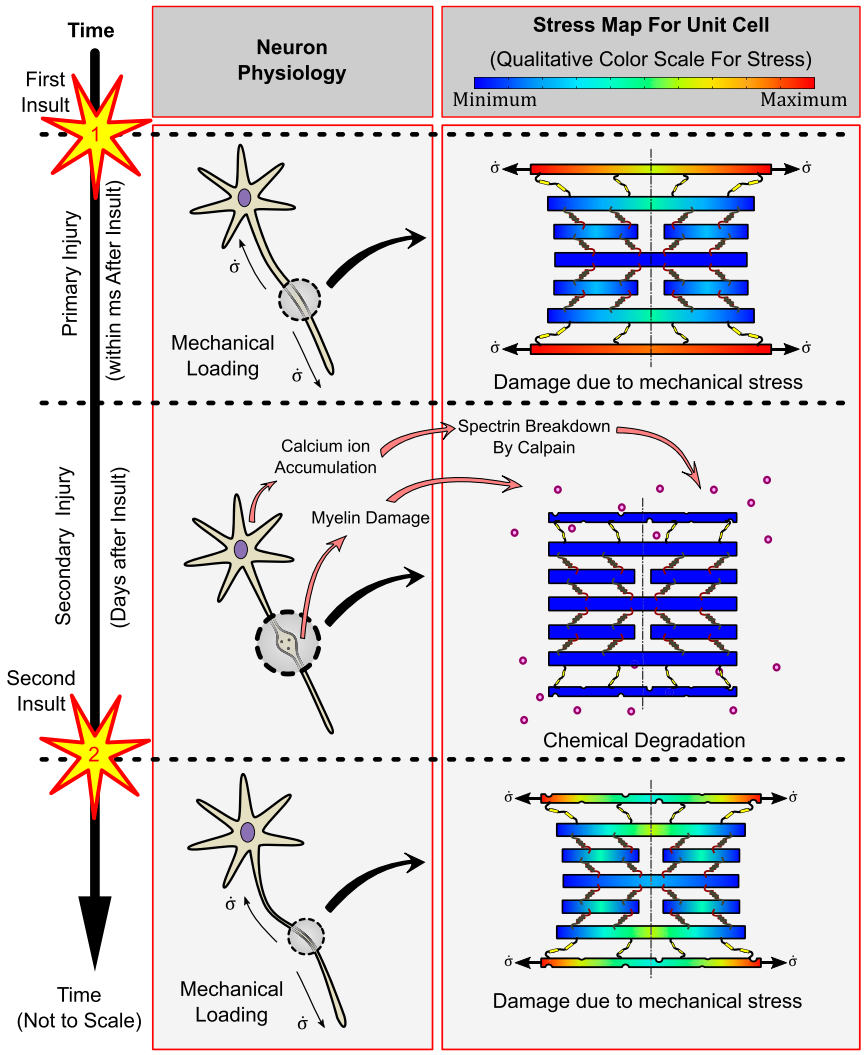

Fig. 6. A schematic diagram summarizing the significant results of the study. Immediately after a brain injury (first insult), the primary injury initiates due to the stress transfer from the cortical cytoskeleton to the MT core. The relatively softer cortex experiences higher stress, effectively shielding the otherwise susceptible MT core. Secondary injuries are seen over a time scale of days to weeks after the first insult wherein calpain activated by intracellular calcium ion accumulation breaks down the cortical spectrin as well as the myelin, rendering it softer. When a second insult occurs, the softer cortex and myelin allow a more significant load transfer to the MTs, making them more susceptible to mechanical stress.

tissue and appears to reveal a distinct subpopulation of degenerating axons undetected by the gold standard immunohistochemical marker of axonal pathology, amyloid precursor protein (14).

Immunohistochemistry specific for SNTF performed in swine brain tissues following a model of mTBI confirms the presence of calpain-mediated spectrin breakdown within injured axons in vivo both here and as described previously (14). Specifically, damaged axons displaying undulated or beaded morphologies exhibited SNTF immunoreactivity acutely after the single mTBI. While SNTF immunoreactivity after single mTBI has been reported previously (14), in this work we report the effects of repeated mTBIs on the in vivo SNTF immunoreactivity of injured axons. In confirmation with our model predictions, our in vivo experiments show that repeated TBIs result in a progressive increase in axon pathology. With the evidence from these observations and having established that the cytoskeletal cortex plays a shielding role for the MT cores in the axon, we establish that the mechanoprotection offered by the cortex is impaired due to secondary degeneration of the cytoskeleton.

In addition to the strong evidence from our swine studies on the altered mechanoprotective behavior of the cytoskeletal components due to their neurodegeneration, in vivo measurements of the temporal progression of neurodegeneration reported in the literature support our model's prediction of axonal vulnerability after mTBI. On a parametric loading space of tissue stress versus the tissue loading rate, our model captures the increasing vulnerability of the axons with time after the first TBI. The increasing unsafe space on the failure plots in Fig. 5 shows how loading parameters at lower tissue stresses and stress rates which were seen to be safe for axons before the first mTBI, are no longer safe if repeated incidences of mTBI occur. In accordance with the experimental observations of Siman et al. (46) we observed a window of vulnerability within which any repeated incidence of mTBI results in a more severe outcome for the axon. Outside this window of vulnerability, when the hockey players can return to play, the recovered axon has a similar unsafe parametric space as for an uninjured axon. A similar window of vulnerability is observed in the experimental reports on the loss of MBP expression in mice brain tissues after mTBI (15). While we have used these different experiments from the reported literature for capturing the loss of mechanoprotective properties of different axonal components like myelin and axonal cortex, we caution that these data are for different subjects and different mechanisms of injury and may not be

suitable for a comparison of neuroprotective capabilities of these components. Thus, our computational model, in conjunction with the experiments reported by us, along with those reported previously in literature, presents a mechanistic understanding for progressive increase in susceptibility of axons to MT rupture in repeated TBIs.

A summary schematic of our results is shown in Fig. 6, showing morphological changes in neurons and corresponding qualitative stress maps due to the chemical injuries following single and repetitive TBIs. Within a time of microseconds to milliseconds after the head impact, mechanical loading of the MT core occurs, referred to as the primary mechanical injury. We have studied in depth the mechanism of load transfer with an emphasis on the roles played by cytoskeletal constitutive parameters in shielding the MTs. While the mechanical stresses during the primary injury stage after the first insult might not be high enough to induce a mechanical failure, its repercussions are seen during the secondary chemical injury stage. Within a few hours after the head impact, significant degradation of myelin and proteolysis of cortical spectrin results in lowering of the elasticity of the myelin-cortex bilayer. The effects of secondary injury may last up to weeks to months after the TBI. Once the second injury occurs, the softer cortex exposes the MT core to a higher load, even if the second insult might be of a magnitude lower than the first. Thus, the second insult and any successive TBI are expected to result in progressively more severe pathology. After a temporary window of vulnerability, potential repair of the axon structure may occur with recovery of myelin and diminished spectrin breakdown. As such, if future TBI were to occur after this window of vulnerability, the resulting mechanical stresses may be better tolerated.

Conclusion

In the long term, our model has potential to be improved with addition of other features to be a viable tool for identifying the potential therapeutics. While our model with a combined myelin and axonal cortex layer still provides accurate predictions, decoupling these into individual layers would allow us to measure their individual contributions to mechanoprotection. A model to this end has been proposed by us in the Supplementary Information. This could be very useful in identifying particular therapeutics for remyelination or preventing spectrin proteolysis at appropriate time periods after an injury. A more detailed study would require a considerable input from experimental data in order to accurately capture the mechanics of load transfer from the myelin wrapping to the axonal cortex and further to the MTs. A detailed analysis of elongation behavior of the family of spectraplakin proteins and their distribution in an axon would allow us to more accurately capture their behavior, improving the accuracy of our model. All of these features can readily be incorporated in the general theoretical framework developed here, primarily by replacing the mechanical elements with more complex models with input from new experiments as they become available. Last, another approach viable in the near future is the effect of local MT disruptions in axons on the macroscale tissue-level mechanotransduction. Such a multiscale study would incorporate a tissue-level spatial heterogeneity not only in the axonal ultrastructure but also in the neurodegenerative effects of secondary injury. Several factors such as the effect of axonal tracts inducing spatially varying anisotropy, heterogeneities in the axonal structures across different regions of the brain, and spatial heterogeneities in the tissue composition itself could be presumed play a significant role here too. Such a study could allow us to predict regions of the brain more susceptible to DAI, especially under repeated TBI conditions.

Our work sheds light on the link between the macroscale tissue strain and its microstructural destabilizing effects. A parametric study of the constitutive behavior of the cytoskeletal components has also led us to a better mechanistic understanding of the role played by secondary chemical injuries in rendering the axon more susceptible to subsequent TBIs. We believe that the phase diagrams predicted by our model can potentially play a significant role in predicting critical axonal loading conditions not only for a single TBI but for repetitive brain injuries. The cytoskeletal load transfer mechanism proposed by us can have applications in suggesting potential cytoskeletal therapeutic targets to alleviate the mechanical stressing of axonal MT assembly, thus preventing its rupture due to incidences of TBI in the future.

Data Availability. All study data are included in the article and/or *SI Appendix*.

ACKNOWLEDGMENTS. We gratefully acknowledge fruitful discussions with Pramod A. Pullarkat and Sushil Dubey (Raman Research Institute, India) with respect to modeling fidelity with their neuron stretch experiments. This work was supported by the Paul Allen Family Foundation; NIH Grants EB021293 (V.B.S. and D.H.S.), NS038104 (D.H.S.), NS094003 (D.H.S.), and NS092398 (D.H.S.); and a Pennsylvania State Commonwealth Universal Research Enhancement (CURE) Award. We thank the NSF Center for Engineering Mechanobiology (Grant CMMI-154857) for the computational resources used in the work and graphics support.

1. S. L. James *et al*.; GBD 2016 Traumatic Brain Injury and Spinal Cord Injury Collaborators, Global, regional, and national burden of traumatic brain injury and spinal cord injury, 1990-2016: A systematic analysis for the Global Burden of Disease Study 2016. *Lancet Neurol.* **18**, 56–87 (2019).
2. J. D. Cassidy *et al*.; WHO Collaborating Centre Task Force on Mild Traumatic Brain Injury, Incidence, risk factors and prevention of mild traumatic brain injury: Results of the WHO Collaborating Centre Task Force on Mild Traumatic Brain Injury. *J. Rehabil. Med.* **36** (suppl.(43) 28–60 (2004).
3. V. E. Johnson, W. Stewart, D. H. Smith, Axonal pathology in traumatic brain injury. *Exp. Neurol.* **246**, 35–43 (2013).
4. R. M. Wright, K. Ramesh, An axonal strain injury criterion for traumatic brain injury. *Biomech. Model. Mechanobiol.* **11**, 245–260 (2012).
5. I. Hahn, A. Voelzmann, Y.-T. Liew, B. Costa-Gomes, A. Prokop, The model of local axon homeostasis—Explaining the role and regulation of microtubule bundles in axon maintenance and pathology. *Neural Dev.* **14**, 11 (2019).
6. M. D. Tang-Schomer, V. E. Johnson, P. W. Baas, W. Stewart, D. H. Smith, Partial interruption of axonal transport due to microtubule breakage accounts for the formation of periodic varicosities after traumatic axonal injury. *Exp. Neurol.* **233**, 364–372 (2012).
7. H. Ahmadzadeh, D. H. Smith, V. B. Shenoy, Viscoelasticity of tau proteins leads to strain rate-dependent breaking of microtubules during axonal stretch injury: Predictions from a mathematical model. *Biophys. J.* **106**, 1123–1133 (2014).
8. H. Ahmadzadeh, D. H. Smith, V. B. Shenoy, Mechanical effects of dynamic binding between tau proteins on microtubules during axonal injury. *Biophys. J.* **109**, 2328–2337 (2015).
9. M. Krieg, A. R. Dunn, M. B. Goodman, Mechanical control of the sense of touch by β-spectrin. *Nat. Cell Biol.* **16**, 224–233 (2014).
10. M. Krieg *et al*., Genetic defects in β-spectrin and tau sensitize *C. elegans* axons to movement-induced damage via torque-tension coupling. *eLife* **6**, e20172 (2017).
11. J. R. Kulbe, E. D. Hall, Chronic traumatic encephalopathy-integration of canonical traumatic brain injury secondary injury mechanisms with tau pathology. *Prog. Neurobiol.* **158**, 15–44 (2017).
12. S. Mondello *et al*., αII-spectrin breakdown products (SBDPs): Diagnosis and outcome in severe traumatic brain injury patients. *J. Neurotrauma* **27**, 1203–1213 (2010).
13. H. Zetterberg, D. H. Smith, K. Blennow, Biomarkers of mild traumatic brain injury in cerebrospinal fluid and blood. *Nat. Rev. Neurol.* **9**, 201–210 (2013).
14. V. E. Johnson *et al*., SNTF immunostaining reveals previously undetected axonal pathology in traumatic brain injury. *Acta Neuropathol.* **131**, 115–135 (2016).
15. T. Taib *et al*., Neuroinflammation, myelin and behavior: Temporal patterns following mild traumatic brain injury in mice. *PLoS One* **12**, e0184811 (2017).
16. T. M. Reeves, L. L. Phillips, J. T. Povlishock, Myelinated and unmyelinated axons of the corpus callosum differ in vulnerability and functional recovery following traumatic brain injury. *Exp. Neurol.* **196**, 126–137 (2005).
17. J. Weickenmeier *et al*., Brain stiffness increases with myelin content. *Acta Biomater.* **42**, 265–272 (2016).
18. A. J. Mierzwa, C. M. Marion, G. M. Sullivan, D. P. McDaniel, R. C. Armstrong, Components of myelin damage and repair in the progression of white matter pathology after mild traumatic brain injury. *J. Neuropathol. Exp. Neurol.* **74**, 218–232 (2015).
19. M. C. Liu *et al*., Extensive degradation of myelin basic protein isoforms by calpain following traumatic brain injury. *J. Neurochem.* **98**, 700–712 (2006).
20. B. C. Mouzon *et al*., Chronic neuropathological and neurobehavioral changes in a repetitive mild traumatic brain injury model. *Ann. Neurol.* **75**, 241–254 (2014).
21. D. H. Smith, V. E. Johnson, W. Stewart, Chronic neuropathologies of single and repetitive TBI: Substrates of dementia? *Nat. Rev. Neurol.* **9**, 211–221 (2013).

22. D. H. Smith, V. E. Johnson, J. Q. Trojanowski, W. Stewart, Chronic traumatic encephalopathy—Confusion and controversies. *Nat. Rev. Neurol.* **15**, 179–183 (2019).
23. E. G. Takhounts *et al*., Investigation of traumatic brain injuries using the next generation of simulated injury monitor (SIMon) finite element head model. *Stapp Car Crash J.* **52**, 1–31 (2008).
24. H. Kimpara, M. Iwamoto, Mild traumatic brain injury predictors based on angular accelerations during impacts. *Ann. Biomed. Eng.* **40**, 114–126 (2012).
25. S. J. Peter, M. R. Mofrad, Computational modeling of axonal microtubule bundles under tension. *Biophys. J.* **102**, 749–757 (2012).
26. R. de Rooij, K. E. Miller, E. Kuhl, Modeling molecular mechanisms in the axon. *Comput. Mech.* **59**, 523–537 (2017).
27. R. de Rooij, E. Kuhl, Microtubule polymerization and cross-link dynamics explain axonal stiffness and damage. *Biophys. J.* **114**, 201–212 (2018).
28. W. Yu, P. W. Baas, Changes in microtubule number and length during axon differentiation. *J. Neurosci.* **14**, 2818–2829 (1994).
29. D. A. Dillard, "Fundamentals of stress transfer in bonded systems" in *Adhesion Science and Engineering*, D. A. Dillard, A. V. Pocius, M. Chaudhury, Eds. (Elsevier, Amsterdam, 2002), pp. 1–44.
30. S. Suresh, Biomechanics and biophysics of cancer cells. *Acta Biomater.* **3**, 413–438 (2007).
31. S. Wegmann, J. Schöler, C. A. Bippes, E. Mandelkow, D. J. Muller, Competing interactions stabilize pro- and anti-aggregant conformations of human tau. *J. Biol. Chem.* **286**, 20512–20524 (2011).
32. E. Bar-Kochba, M. T. Scimone, J. B. Estrada, C. Franck, Strain and rate-dependent neuronal injury in a 3D in vitro compression model of traumatic brain injury. *Sci. Rep.* **6**, 30550 (2016).
33. N. Snaidero, M. Simons, The logistics of myelin biogenesis in the central nervous system. *Glia* **65**, 1021–1031 (2017).
34. R. H. Quarles, Myelin-associated glycoprotein (MAG): Past, present and beyond. *J. Neurochem.* **100**, 1431–1448 (2007).
35. R. Siman, C. Zhang, V. L. Roberts, A. Pitts-Kiefer, R. W. Neumar, Novel surrogate markers for acute brain damage: Cerebrospinal fluid levels correlate with severity of ischemic neurodegeneration in the rat. *J. Cereb. Blood Flow Metab.* **25**, 1433–1444 (2005).
36. R. Siman *et al*., Proteins released from degenerating neurons are surrogate markers for acute brain damage. *Neurobiol. Dis.* **16**, 311–320 (2004).
37. R. Siman *et al*., A panel of neuron-enriched proteins as markers for traumatic brain injury in humans. *J. Neurotrauma* **26**, 1867–1877 (2009).
38. R. Siman, D. G. Flood, G. Thinakaran, R. W. Neumar, Endoplasmic reticulum stress-induced cysteine protease activation in cortical neurons: Effect of an Alzheimer's disease-linked presenilin-1 knock-in mutation. *J. Biol. Chem.* **276**, 44736–44743 (2001).
39. J. M. Roberts-Lewis, M. J. Savage, V. R. Marcy, L. R. Pinsker, R. Siman, Immunolocalization of calpain I-mediated spectrin degradation to vulnerable neurons in the ischemic gerbil brain. *J. Neurosci.* **14**, 3934–3944 (1994).
40. M. C. Holley, J. F. Ashmore, Spectrin, actin and the structure of the cortical lattice in mammalian cochlear outer hair cells. *J. Cell Sci.* **96**, 283–291 (1990).
41. S. N. Ricketts *et al*., Varying crosslinking motifs drive the mesoscale mechanics of actin-microtubule composites. *Sci. Rep.* **9**, 12831 (2019).
42. D. C. Viano, I. R. Casson, E. J. Pellman, Concussion in professional football: Biomechanics of the struck player—Part 14. *Neurosurgery* **61**, 313–327, discussion 327–328 (2007).
43. G. S. Nusholtz, P. Lux, P. Kaiker, M. A. Janicki, Head impact response—Skull deformation and angular accelerations. *SAE Trans.* **93**, 800–833 (1984).
44. S. Dubey *et al*., The axonal actin-spectrin lattice acts as a tension buffering shock absorber. *eLife* **9**, e51772 (2020).
45. V. E. Johnson *et al*., Mechanical disruption of the blood-brain barrier following experimental concussion. *Acta Neuropathol.* **135**, 711–726 (2018).
46. R. Siman *et al*., Serum SNTF increases in concussed professional ice hockey players and relates to the severity of postconcussion symptoms. *J. Neurotrauma* **32**, 1294–1300 (2015).
47. J. Kim *et al*., Mechanical stretch induces myelin protein loss in oligodendrocytes by activating Erk1/2 in a calcium-dependent manner. *Glia* **68**, 2070–2085 (2020).
48. V. E. Johnson *et al*., Inflammation and white matter degeneration persist for years after a single traumatic brain injury. *Brain* **136**, 28–42 (2013).
49. C. C. Bruce, C. Zhao, R. J. Franklin, Remyelination—An effective means of neuroprotection. *Horm. Behav.* **57**, 56–62 (2010).
50. O. Farkas *et al*., Spectrin breakdown products in the cerebrospinal fluid in severe head injury—Preliminary observations. *Acta Neurochir. (Wien)* **147**, 855–861 (2005).
51. C. S. Hill, M. P. Coleman, D. K. Menon, Traumatic axonal injury: Mechanisms and translational opportunities. *Trends Neurosci.* **39**, 311–324 (2016).
52. M. Hammarlund, E. M. Jorgensen, M. J. Bastiani, Axons break in animals lacking β-spectrin. *J. Cell Biol.* **176**, 269–275 (2007).